The Design and Fabrication of a Passive and Continuously Repositionable Joint

by

Phillip H. Daniel

SUBMITTED TO THE DEPARTMENT OF MECHANICAL ENGINEERING IN PARTIAL FULFILLMENT OF THE REQUIREMENTS FOR THE DEGREE OF

BACHELOR OF SCIENCE IN MECHANICAL ENGINEERING
AT THE
MASSACHUSETTS INSTITUTE OF TECHNOLOGY

JUNE 2013

Signature of Author: _____
Department of Mechanical Engineering
May 17, 2013

Certified by: _____
Alexander H. Slocum
Pappalardo Professor of Mechanical Engineering
Thesis Supervisor

Accepted by: _____
John H. Lienhard V
Collins Professor of Mechanical Engineering
Chairman, Undergraduate Thesis Committee

The Design and Fabrication of a Passive and Continuously Repositionable Joint

by

Phillip H Daniel

Submitted to the Department of Mechanical Engineering
on May 17, 2013 in Partial Fulfillment of the
Requirements for the Degree of Bachelor of Science in
Mechanical Engineering

ABSTRACT

A cam based locking mechanism was designed and fabricated to secure the joints of a continuously repositionable table capable of supporting a 111N load. Additionally, a frame was designed and built to test the feasibility of this joint concept as an assembly. Conventional toothed mechanisms were found to not provide a desirable smoothness of motion or resolution for implementation as an adjustable table. They also require more geometrically complex components than the proposed solution. The proposed mechanism relies on the binding of an eccentric cam and pulley, and is of interest because these key components are geometrically simple in comparison to toothed mechanisms. The reduced complexity of this solution is expected to lower the manufacturing cost of this type of joint and increase the resolution of its angular position, when compared to similar mechanisms.

A model of the jamming interaction was evaluated using Matlab. This model was used to select the optimal material, eccentricity and diameter of the components. The elements were then fabricated with an Omax 2626 Precision JetMachining Center, and mechanically tested using calibrated weights. The fabricated joint is capable of holding a 56.5N*m load with a stiffness of 7.8N*m/degree.

Thesis Supervisor: Alexander H. Slocum
Title: Pappalardo Professor of Mechanical Engineering

Contents

List of Figures and Tables

1. Introduction

In the consumer market there are numerous adjustable tables/stands. However, these products either have a limited number of discrete positions and can support a heavy load, akin to standing desks (178 N), or they are easily adjustable but can support only light loads, e.g. computer monitor mounts (22 N). Additionally, heavy duty mounts are generally difficult to adjust and are semi-permanently assembled at a user's desired position, and light duty mounts are generally unable to support physical interaction with a user such as typing.

One demographic that suffers from these trends is endurance cyclists. Such athletes train for multiple hours at a time on stationary bikes, but are not able to easily do other work simultaneously. This is because of the lack of existence of an easily adjustable stand that can position their personal items (e.g. laptop, tablet, etc.) as they transition between different cycling postures.

To solve this problem, work was done to design a joint for an adjustable stand that will allow bicycle athletes to easily position and use their personal items, by stiffly supporting the loads associated with user interaction. (Figure 1)

Figure 1: This shows the final joints assembled into a frame. This prototype was used to evaluate the feasibility of the joint concept.

The joint functions by taking advantage of the nonlinear increase in resisting torque as jamming elements rotate through a marginally stable toggle point. To function reliably as intended, the main components must be able to withstand the forces resulting from repetitive

use without being permanently deformed. This resilience was considered in the model, and tested through the application of calibrated loads.

2. Background of Jamming Cams

A cam's ability to transmit load through jamming is a feature that is exploited in many tools. Most notably, this feature is exploited by active climbing nuts such as those pictured in Figure 2.

Figure 2: The left set of images (Sam, 2012) show an active climbing nut deployed (left) and retracted (center). The right most image (John, 2011) shows a retracted climbing nut deployed in a crack and loaded through a cable.

The jamming caused by the increasing radius of the cams is used to wedge the climbing nut into cracks. The load through the cable that is attached to the nut deploys the cams against the walls of its crack with a significant mechanical advantage. The resulting force between the cams and the crack they are wedged in is high enough to support a person's body weight with friction. This is the core functionality of the cam used in the proposed joint, only now the surface interacting with the cam is a circular pulley instead of a linear crack.

3. Design of a Jam Locking Joint

The proposed mechanism locks in position when the two main elements come in contact with each other and statically jam. This jamming occurs because the distance between the axis of rotation of both elements, D, is smaller than sum of the maximum radii of the components. When the compressive force at the contact point between the cam and the pulley, F_{comp}, causes a reaction torque, T_{resist}, large enough to resist the loading torque, the joint is considered locked.

Most feasible materials for the elements have a modulus of elasticity, E, low enough to allow the jamming force between the elements to also cause them to undergo strain deformation. When this occurs, the components rotate with respect to each other, θ_2, until the compressive force between them is high enough to resist the loading torque. (Figure 3)

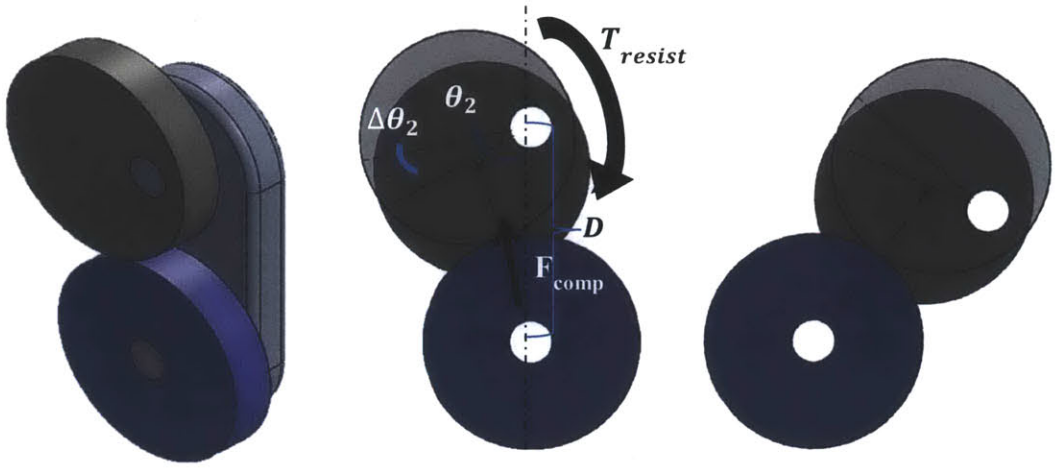

Figure 3: The image on the left shows the elements before jamming has occurred. The image in the center shows a front view of elements interfering. Finally, the image on the right shows the elements interfering at a different position along the pulley (blue). To aid in depicting the interaction, the pulley is shown to be undergoing no deformation and the cam has an exaggerated eccentricity.

The figure shows the jamming interaction of the elements. The pulley is round because this allows the same jamming interaction to occur anywhere along its surface. This is the feature that allows the joint to position load along a continuous range of angles.

The angular displacement of the cam from contact to static equilibrium, $\Delta\boldsymbol{\theta_2}$, and the desired holding torque of the joint, T_{resist}, set by the functional requirements of the joint's implementation, define the joint's necessary stiffness,

$$K_{joint} = \frac{T_{resist}}{\Delta\theta_2}. \quad (1)$$

3.1 Overview of Joint Interaction Modes

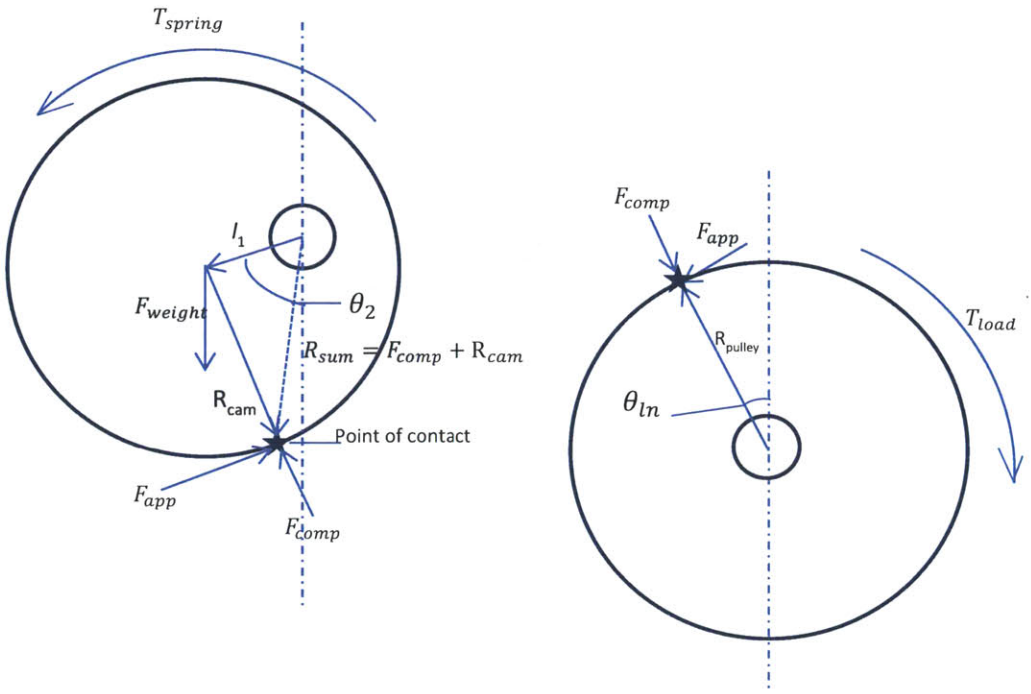

Figure 4: This is a free body diagram of the pulley (left) and the cam (right).

There are three types of interactions between the eccentric cam and the pulley, rolling-jamming without sliding, rolling-jamming with sliding, and sliding. Rolling-jamming without sliding is when there is no relative motion between the cam and the pulley, and the elements are engaged like gear teeth. Rolling-jamming with sliding is when the elements are in engaged but also slipping. Here, the coefficient of dynamic friction is high enough to transmit load between the cam and the pulley and compress the elements. Finally, sliding is when the two elements slip with respect to each other, and the coefficient of dynamic friction isn't high enough to transmit sufficient load to compress the elements.

Rolling-jamming without sliding will occur when and while the sum of the loading torque on the cam, $T_{load,2}$, from frictional contact with the pulley, F_{app}, and the torque from the preloading spring and weight, T_{spring} and F_{weight}, are greater than or equal to the resisting torque on the cam, T_{resist}. T_{resist} is the reaction torque on the cam from the compression of the two elements. This is represented as,

$$T_{load,2} + T_{spring} > T_{resist}, \tag{2}$$

where $T_{load,2}$ is proportional to the radius of the cam, R_{cam}, and its offset, l_1, based on the equation

$$T_{load,2} = (R_{cam} + l_1) \times F_{app,} \quad (3)$$

where,

$$F_{app} = T_{load}/R_{pulley}. \quad (4)$$

T_{resist} is proportional to the offset of the cam, l_1, according to

$$T_{resist} = (R_{cam} + l_1) \times F_{comp}. \quad (5)$$

Also, it must be the case that the maximum force of static friction, $F_{fric,static}$, is greater than or equal to the applied frictional force on the cam,

$$F_{fric,static} \geq F_{app}, \quad (6)$$

where,

$$F_{fric,static} = \mu_{static} * F_{comp}. \quad (7)$$

The elements will be at static equilibrium when the above is true, and when

$$T_{load,2} + T_{spring} = T_{resist}. \quad (8)$$

Rolling-jamming with sliding will occur when the loading torque from the pulley results in a higher force at the interface than static friction can support, but when the moment, T_{slide}, from the force of dynamic friction, $F_{fric,dynamic}$, summed with the moment from the spring is enough to overcome the resisting torque,

$$T_{slide} + T_{spring} \geq T_{resist}, \quad (9)$$

where,

$$T_{slide} = (R_{cam} + l_1) \times F_{fric,dynamic} \quad (10)$$

Here, because the elements are sliding and jamming, static equilibrium will only be reached once the conditions of Equations 6 & 8 are achieved. This will occur if the maximum force of static friction increases to above the applied frictional force on the cam, as a result of the compressive force between the elements increasing.

If neither of the above criteria is satisfied, then jamming will not occur. Instead, the two surfaces will slip against each other indefinitely.

3.2 Model of Rolling-Jamming Without Sliding

The resisting torque is a function of the compressive force between the elements, F_{comp}, directed along the line of action through each element's center, the offset vector on the cam, l_1, and the radial vector from the cam's geometric center to the point of contact, as defined in Equation 5. To fully model the interaction, a moment balance was evaluated at the pin in the cam. This resulted in the equation

$$\sum M_{pin} = (l_1 \times F_w) + (R_{sum} \times F_{app}) + (R_{sum} \times F_{comp}) + T_{spring} = 0. \quad (11)$$

To evaluate this expression, we must first solve for l_1, R_{sum} and F_{comp} in terms of known parameters. We will then use these results to solve for F_{app} by deduction.

The direction of l_1 is θ_2, the direction of F_{comp} is θ_{ln} and the direction of R_{sum} depends on both angles.(Figure 4) Because these angles depend on the deformation of the elements at the point of their interaction, and the function defining this deformation couldn't be easily manipulated into a simple function of θ_2 or θ_{ln}, these values were determined implicitly, as described below.

To approximate F_{comp} as a function of the compressed length between the elements, the analysis from the paper, "Elastic Compression of Spheres and Cylinders as Point and Line Contact" was used. (Puttock & Thwaite, 1969) This provided an expression for the amount of elastic compression between two cylinders, α, as a function of F_{comp}. (Figure 5)

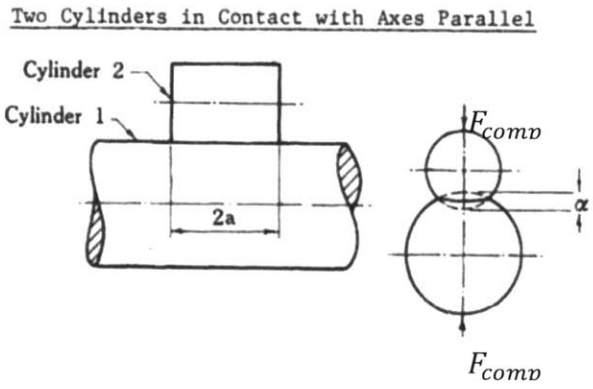

Figure 5: The solution in the referenced literature assumes that the cylindrical elements have forces acting only radially. While this isn't true of the arrangement in the joint lock, the 'misalignment' of the axis is small.

The analysis resulted in the following expression, where a is half the length of the contact region and V is the shear modulus of the material.

$$\alpha = 2 * P_{bar} * V\left(1 + \ln\left(\frac{4*a^2}{V*P_{bar}} * \left(\frac{1}{D_{cam}} + \frac{1}{D_{pulley}}\right)\right)\right), \quad (12)$$

where,

$$P_{bar} = \frac{F_{comp}}{2*a}. \quad (13)$$

Though this solution assumes that all loading forces are acting radially to the components, i.e. no offset, the result was used to approximate the compressive force during the interaction of the elements because the implemented offset is less than 3% of the radius of the cam.

To relate F_{comp} to θ_2 and θ_{ln} to θ_2, a vector of semi-arbitrary compressive forces, F_{comp}, was entered into the above equation using Matlab. The output is a vector of linear compression values, α, which was converted to a vector of values for θ_2 according to the relation

$$\theta_2 = \cos^{-1}\left((R_{pulley} + R_{cam} - \alpha)^2 - l_1^2 - (D)^2\right)/(-2 * (D) * l_1)\,. \tag{14}$$

This above result is based on the geometric decomposition of Figure 4, with the far field assumption that the linear compression of the elements only distorts the vectors R_{cam} and R_{pulley}, but not l_1. We then convert the vector of θ_2 values to a vector of θ_{ln} values with a second vector decomposition,

$$\theta_{ln} = \tan^{-1}(l_1 * \sin(\theta_2)/((D) - l_1 * \cos(\theta_2)). \tag{15}$$

Once vectors for F_{comp}, α, θ_2 and θ_{ln} are obtained, the cross products of Equation 11 can be evaluated and solved for F_{app} as,

$$F_{app} = \frac{T_{spring} + l_1 * F_{weight} * \sin(\theta_2) - l_1 * F_{comp} * \sin(\theta_2 + \theta_{ln})}{l_1 * \cos(\theta_2 + \theta_{ln}) - R_{cam} + \alpha}. \tag{16}$$

The final step in characterizing the mode of jamming is to evaluate the maximum force of static friction and the dynamic force of friction. The coefficients were estimated initially, and then measured with an inclined plane test of the fabricated surfaces. The forces were evaluated as

$$F_{fric,static} = u_{static} * F_{comp}, \tag{17}$$

$$F_{fric,dynamic} = u_{kinetic} * F_{comp}. \tag{18}$$

Equation 17 is now fully defined and the mode of jamming can be evaluated. However, the expression cannot be used for design until the failure mode of the elements is considered.

3.3 Stress Analysis and Evaluation of Design Parameters

The contact stress and compressive strain between the elements may cause the material to fail in shear through plastic deformation. If such deformation occurs, the expression for F_{comp} would become invalid as Equation 12 is intended to only predict forces in the material's elastic regime. In addition to the forces being more difficult to predict, the deformation would alter the shape of the elements and therefore the stiffness of the joint.

To ensure that the joint operates in a repeatable manner and as expected, the Hertz contact stress at the static equilibrium position, $\sigma_{shear,equil}$, was evaluated, along with the strain of each of the elements, ϵ_{equil}, where v is the Poisson ratio of steel. (Slocum, 2007)

$$\sigma_{shear,equil} = .6 * \frac{F_{comp,jam}}{\pi * b * 2 * a} \tag{19}$$

$$\epsilon_{equil} = \alpha/(.5 * R_{pulley} + .5 * R_{cam}), \tag{20}$$

where,

$$b = \sqrt{\frac{8*F_{comp,jam}*R_{cam}*R_{pulley}}{\pi*2*a*E_{equiv}(2*R_1+2*R_2)}} \tag{21}$$

$$E_{equiv} = \frac{E}{2} * (1 - v^2). \tag{22}$$

ϵ_{equil}, $\sigma_{shear,equil}$ and $\theta_{2,equil}$ were then plotted against a range of l_1 values to determine an optimal value of l_1 that results in the stiffest joint. The optimal value of l_1 results in $\epsilon_{equil} \leq .003$, $\sigma_{shear,equil} \leq 345$Mpa, and $\theta_{2,equil} \leq 1°$, for stainless steel elements. Additionally, F_{app} must remain less than $F_{fric,static}$ for $\theta_{2,equil} \leq \theta_2 \leq \theta_{2,initial}$. Under these conditions, the optimal offset was determined to be 3.1mm, given a D of 63.5mm and a thickness of 12.7mm.

Once the optimal offset was determined, the applied friction force between the elements and the maximum force of static friction were plotted against the jamming angle, $\Delta\boldsymbol{\theta_2}$, for the full range of the joint, from $\boldsymbol{\theta_{2,initial}}$ to $\mathbf{0}$. (see Figure 6)

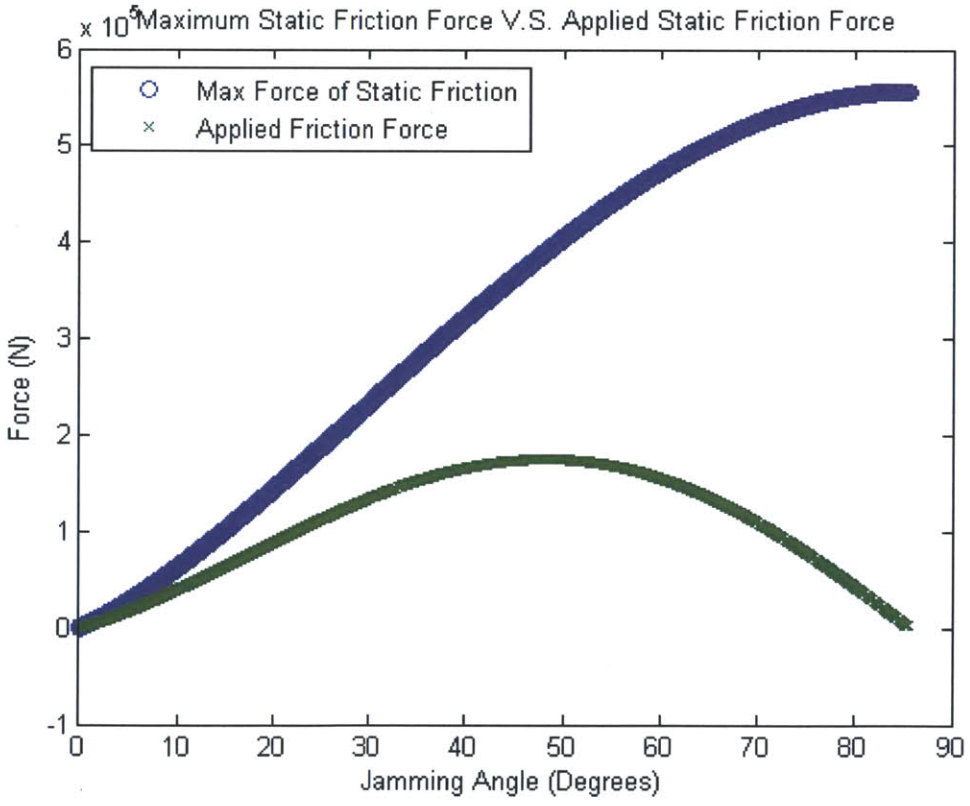

Figure 6: This figure compares the applied frictional force to maximum force that static friction can support. This shows that once the joint begins jamming, the maximum force that static friction can support will always be greater than the applied frictional force.

From Figure 6, it can be seen that jamming is expected persist throughout the motion of the elements during their elastic compression. This is observed from the fact that the applied force of friction doesn't exceed the load that static friction can support at any time during its elastic range of motion.

4. Measurement of Joint Stiffness

4.1 Fabrication of Tested Elements

To test the analytical results for the stiffness of the cams, a set of elements was fabricated using an Omax 2626 Precision JetMachining Center, (Figure 7) according to the parameters reported in Table 1.

Figure 7: This figure shows the elements that were fabricated using the Omax JetMachining Center.

Table 1: Parameters of the fabricated elements.

Cam Radius (mm)	31.75	Radius of pulley (m)	31.75
Thickness of cam (mm)	12.7	Young's Modulus (Pa)	1.93E+11
Thickness of pulley (mm)	12.7	Poisson Ratio	0.305
Offset between joint and center of the cam (mm)	3.1	Distance between axis of rotation of the elements (mm)	63.652
Cam/Pulley pin diameter (m)	12.7	Cam/Pulley Pin Young's Modulus (Pa)	1.93E+11

Before the elements were fabricated, a test part was machined out of the same material to be used in the main components. This allowed the offset of the waterjet to be accurately adjusted. Figure 8 shows the test geometry.

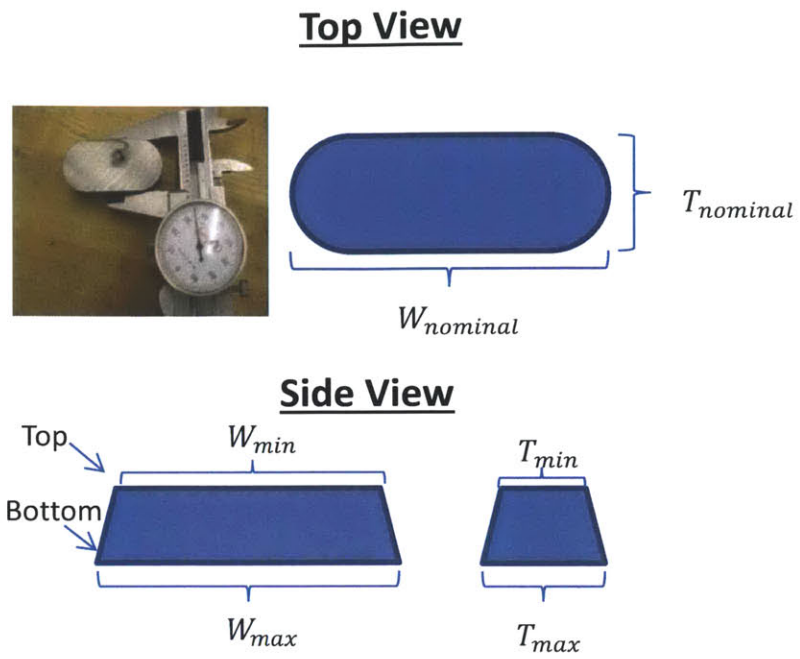

Figure 8: The test geometry was designed so that the taper of the waterjet could be measured for both curved and straight sections.

The offset was determined by measuring the taper between the top and bottom surface of the test geometry, and adjusting the waterjet's default offset so that the minimum dimension of the finished part (on the top side) matched the nominal dimension. The default offset of the waterjet caused the dimensions of the test part to be undersized by ~.2mm. The minimum dimension of the curved section was the most undersized dimension, with a radial error of .216mm under the nominal dimension. The offset was increased by this radial error before the elements were machined.

After fabrication, the diameters of the main elements were measured with calipers and the radial taper resulting from the water jet was found to vary from $3.81*10^{-5}$m (top) to $5.08*10^{-5}$m (bottom) over the elements' nominal dimension. Also, the taper was observed to be "U" shaped as seen in Figure 9.

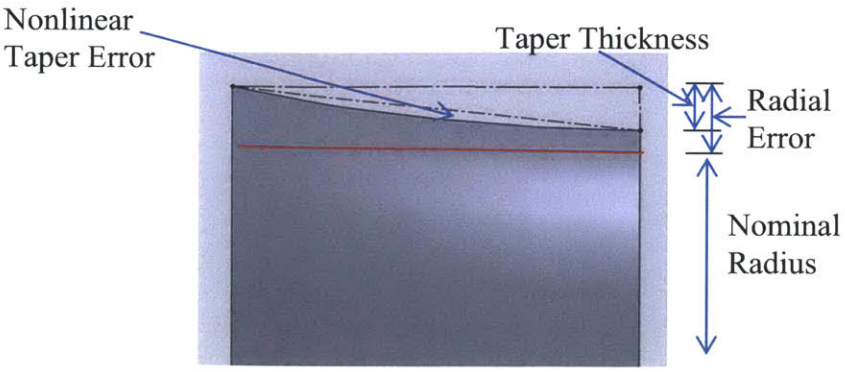

Figure 9: This figure illustrates the maximum and minimum deviation of the cam's machined radius from its nominal radius. The figure also depicts a rendition of the taper between the elements, although this was not explicitly measured.

Although the full geometry of the taper between the major and minor diameter of the parts was not measured, the taper's thickness was measured to be a maximum of $1.27*10^{-5}$m. This permits at most .46 degrees of low stiffness rotation before the taper on both elements is fully compressed.

4.2 Design and Fabrication of Test Apparatus

In addition to fabricating the elements, a frame was built to position and load them during testing and to be used as part of a trial positioning table, see Figure 10.

Figure 10: This shows the frame that was built to position and load the elements. The key components are labeled.

The joint hole in the cam was reamed to a FN 12 fit (ERIK OBERG, 2012) with an Oilite brass bushing. This bushing rested on a 12.7mm steel shoulder bolt, with $5.08*10^{-5}$m of diametrical clearance between the bolt and the bushing. This bolt was fit into bushings at both

ends, with the same press fit to the frame as previously mentioned and the same clearance. The pulley rested directly on a 12.7mm steel bolt with a RC 42 fit (ERIK OBERG, 2012), and was bolted to the joint's support walls with SAE Grade 5 bolts, see Figure 10.

Analysis was done assuming both rigid and flexible shoulder bolts in series with the cam, to bound the expected joint stiffness. For the flexible bolt analysis, the pulley was assumed to be unbolted from the frame and purely supported by its shoulder bolt. While the pulley is supported by the three ¼ 20 bolts holding it to the frame, the bolts used during testing were unable to support the pulley load even when properly preloaded. This is because when torqued, T, to the appropriate torque specification, 21N*m, the preload force, F_i, equals $10.8*10^3$N on each bolt. This preload force equates to a maximum force of static friction equal to $6.6*10^3$N, which is less than the maximum force loading the pulley, 18.4 $*10^3$N. (eFunda Inc., 2013)(Equations 23-25)

$$F_i = .9 * A_t * S_p \tag{23}$$

$$T = K * F_i * d \tag{24}$$

$$F_{fric} = F_i * \mu_s \tag{25}$$

Table 2: Parameters for the bolted joint calculations.

Tensile stress area, A_t	$2.1*10^{-5}m^2$
Proof strength, S_p	$5.86*10^8$Pa
Nominal diameter, d	6.35mm
Coefficient based on the bolt material, K	.3
Coefficient of static friction, μ_s	.61

The stiffness of the shoulder bolts was calculated using beam bending theory, (Craig, 2009) assuming that the shoulder bolts were configured as shown in Figure 11.

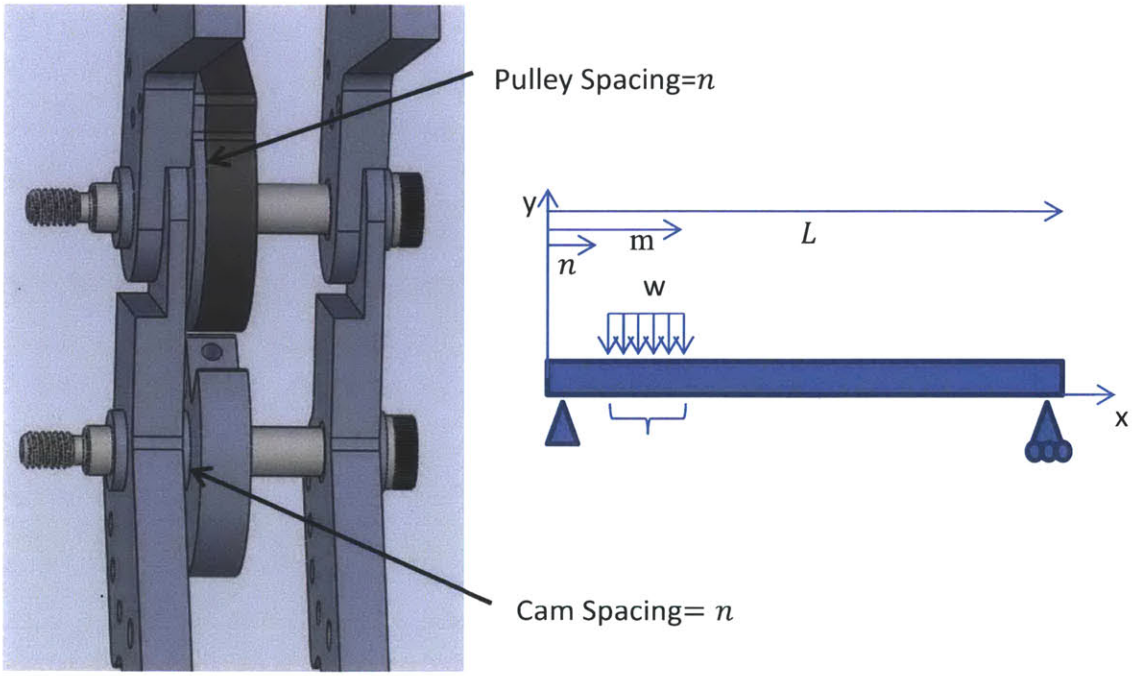

Figure 11: The layout of the shoulder bolt as a beam, for analysis. "n" is the gap between the elements and the assembly wall, "m" is the distance between the far edge of the pulley/cam and the wall, "L" is the effective length of the bolt, and "w" is the force per unit length on the bolt.

Analysis was carried out for a simply supported beam with an even load distribution, because the angle of the shoulder bolts' ends aren't constrained by their running fit with the bushings. The displacement of the bolt in the bushing was checked, and at a max displacement of .02mm inside the bushing, they are known to not interfere. The stiffness of the bolt was taken as the beam stiffness at x = m. The linear stiffness was calculated according to Equation 26, and found to be $1.6 * 10^8$N*m.

$$k_{bolt} = \frac{24\mathrm{LEI(m-n)}}{-\mathrm{n}^4*\mathrm{L}+4\mathrm{L}^2\mathrm{mn}^2+\mathrm{n}^4\mathrm{m}-6\mathrm{Lm}^2\mathrm{n}^2+2\mathrm{m}^3\mathrm{n}^2-\mathrm{m}^4\mathrm{L}+4\mathrm{L}^2\mathrm{m}^3+\mathrm{m}^5-6\mathrm{Lm}^4+2\mathrm{m}^5} \quad (26)$$

4.3. Torque and Displacement Measurement of Assembled Joint

To measure the angular stiffness of the elements, the joint was clamped to a horizontal surface and weights were hung from it in 11N increments, corresponding to a torque load from 0 to 23N*m. During loading, the linear displacement of the joint was measured and used to calculate the angular displacement. (See Figure 12)

Figure 12: The arrangement of the joint during testing.

After the stiffness of a single joint was measured, three elements were assembled in series as a prototype positioning table and the repositionability and torque limit of the stand was tested. In the repositionability test, the orientation of the stand was repeatedly changed and load was applied through typical user interaction. (Figure 13)

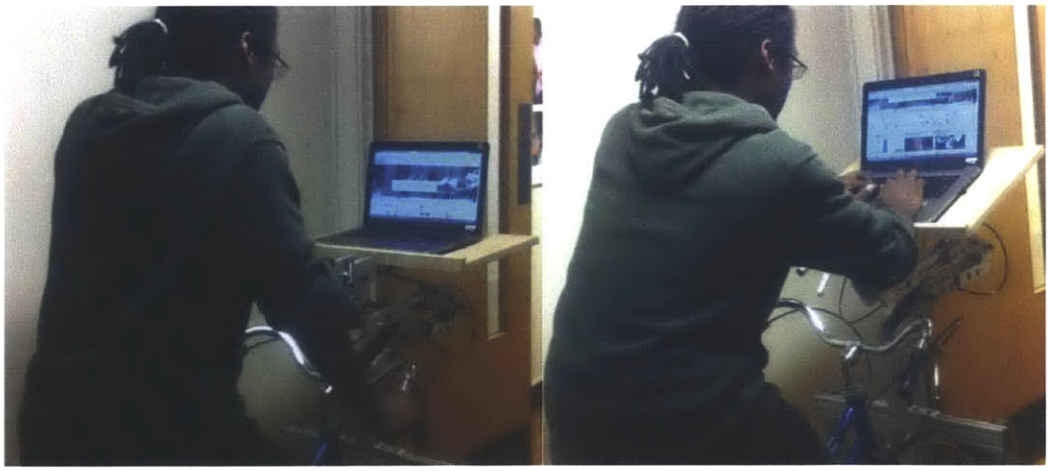

Figure 13: This shows a typical user changing the position of the stand to comfortably interact with it while biking. In the second image, the user is leaning on the stand to support his weight as he types.

The stand was easily repositioned, and rigidly supported user interaction in every orientation.

Next, to test the stand's load limit 111N was placed on the tabletop while each joint was arranged to maximize its resisting torque. This weight corresponded to a 45N*m torque load, plus an additional 18N*m of load for the weight of the stand at the lowest joint. (Figure 14)

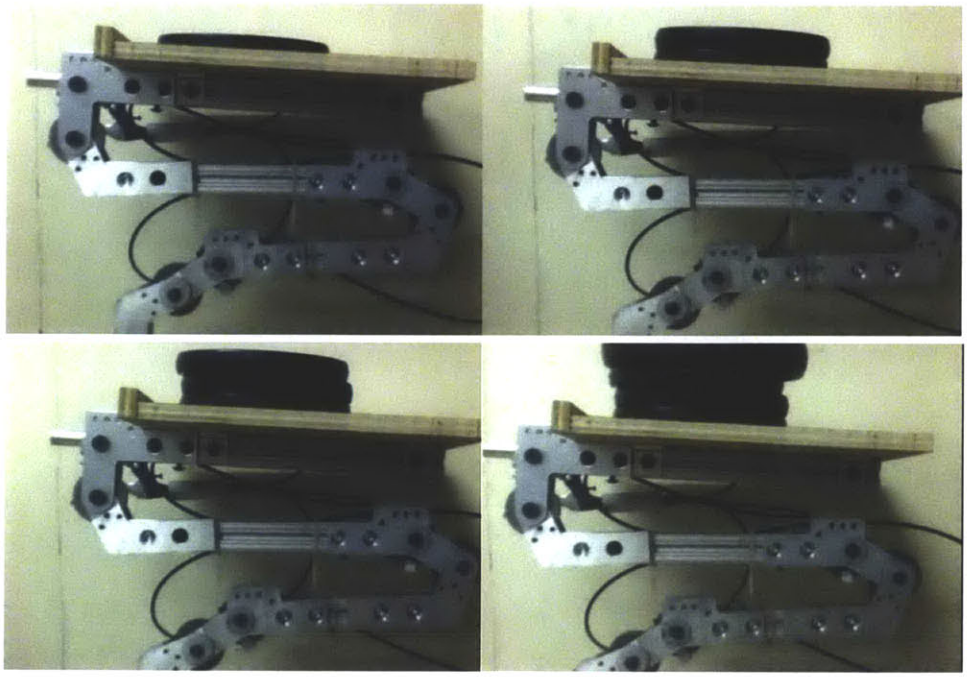

Figure 14: This figure shows the stand during each stage of the load limit test. The assembly was able to rigidly support load corresponding to the elastic limit of the elements.

In this test the elements were loaded to their elastic limit, but didn't fail to rigidly support the load nor did they slip.

5. Results and Discussion

The resisting torque of the fabricated elements was measured and plotted alongside their analytical prediction. Initially, the shoulder bolts were assumed to be rigid. This resulted in an analytical, angular stiffness of 102N*m/degree, compared to a measured angular stiffness of 7.2N*m/degree, see Figure 15.

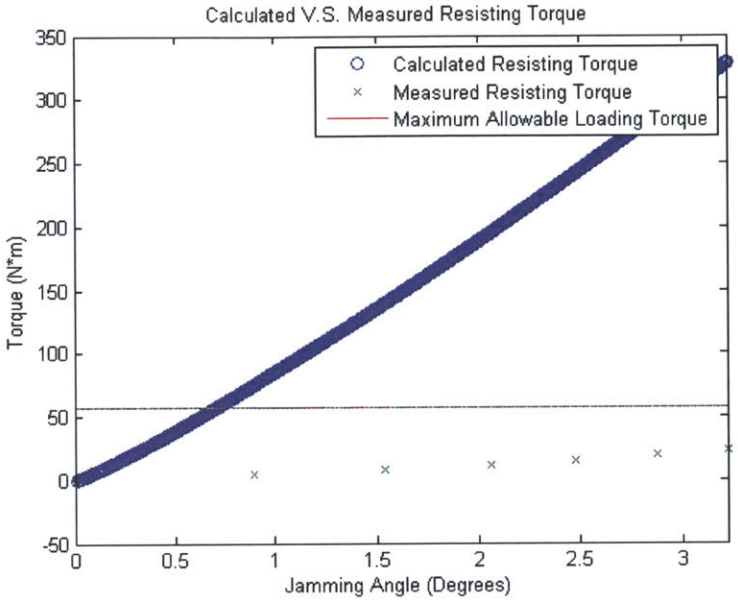

Figure 15: This figure compares the analytical and measured torque loads that the joint supports as a function of the jamming angle, $\Delta\theta_2$. From this, the difference between the measured and expected stiffness can be seen.

Because of the discrepancy between the expected and actual joint stiffness, the analysis was also completed assuming that both the cam and pulley transmitted their loads directly to their shoulder bolts, i.e. the pulley was assumed to be unbolted.

To evaluate the system with compliant shoulder bolts, K_{bolt}, the bolts were assumed to act like springs in series with the cam and pulley stiffness, $K_{cam\&pulley}$. To complete this analysis, the analytical cam and pulley stiffness, derived from Equation 12 was linearized over $0 \leq \Delta\theta_2 \leq \theta_{2,equil} = 3.2$, and Equation 12 was replaced with

$$F_{comp} = K_{assm} * \alpha, \tag{27}$$

Where,

$$K_{assm} = \frac{K_{cam\&pulley} * K_{bolt}}{2 * K_{cam\&pulley} + K_{bolt}}. \tag{28}$$

The analysis was run once again and resulted in an analytical stiffness of 12N*m/degree for the joint. (Figure 16)

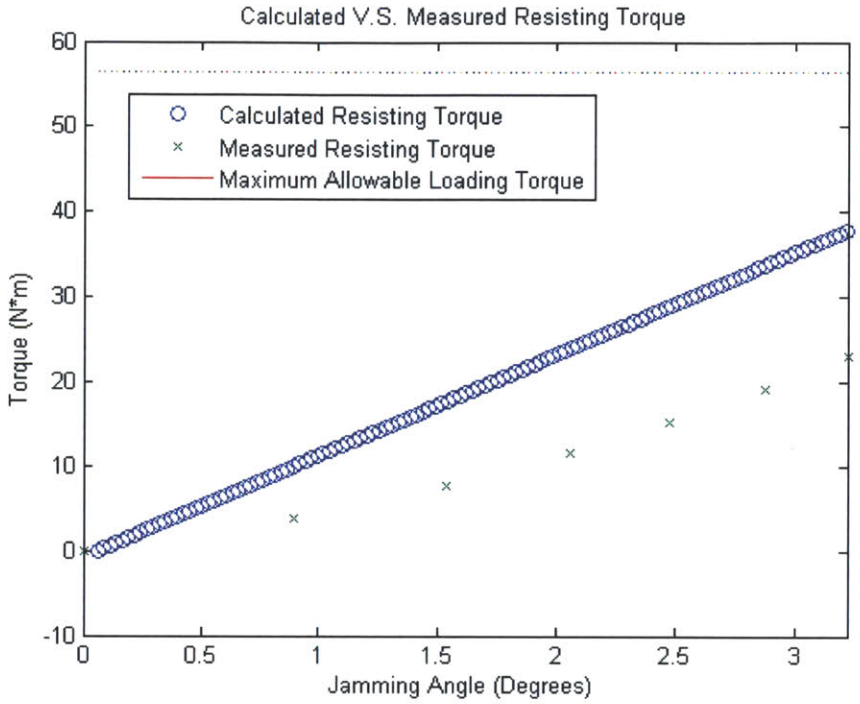

Figure 16: The resisting torque verses the jamming angle, now assuming that both bolts are compliant.

The analytical stiffness is still greater than the measured result however acceptably so, as both values are within only a few Newton-meters of each other. This corresponds to a 7.6N discrepancy in the frames load during testing, which can be reasonably attributed to measurement error or poorly calibrated test weights.

This analysis informs the design of the next iteration of this joint. To bolt the pulley to the frame, the current bolts will be replaced with higher grade steel bolts. This will allow them to be preloaded enough to support the compressive load of the elements, increasing the stiffness of the joint. Additionally, the cam's interface with the frame will be redesigned so that the shoulder bolt supporting it is press-fit into the frame. This will change the end constraints of the bolt to nearly fixed end, and increase its stiffness. Finally, the thickness of the spacer between the cam and the joint wall will be minimized so as to additionally increase the effective stiffness of the bolt. Once these changes are implemented, the measured joint stiffness is expected to increase significantly to better match rigid-bolt analytical stiffness.

6. Conclusion

Jamming without sliding is a robust mode for the kinematics of this joint, an offset cylinder cam with a circular pulley. Additionally, it is feasible to implement this joint in the construction of a rigid positioning table, more specifically for use during endurance-cycling training regiments.

Acknowledgments

The author would like to thank Dr. Alexander Slocum for his guidance throughout the process of setting the scope of the project, selecting the most appropriate joint design, and selecting the most appropriate material and kinematic layout for the frame. The author would also like to thank Dr. Nevan Hanumara for guiding the team to selecting a mechanically sound frame design and for providing invaluable feedback in refining the frame to be both stiff and portable. Additionally, the author appreciates the help of Fulkers Rojas for reviewing the analysis of the joint and helping to guide the design of a stiff frame for the alpha prototype.

The author also appreciates the contributions of Princess Len Carlos for verifying the analysis of the joint, designing and fabricating the unlocking mechanism for the frame, and assisting in the fabrication and assembly of the frame. Finally, the author appreciates the contributions of Netia McCray for refining the kinematic layout of the frame to be ergonomically viable, and for assisting in the final assembly of the stand.

Bibliography

Craig, R. R. (2009). Deflections and Slopes of Beams; Fixed-End Actions. In R. R. Craig, *Mechanics of Materials* (pp. E-3). New York: John Wiley & Sons.

eFunda Inc. (2013). *Torque and Tension in Bolts*. Retrieved May 17, 2013, from eFunda: http://www.efunda.com/designstandards/screws/fasteners_intro.cfm

ERIK OBERG, F. D. (2012). Machinery's Handbook. In F. D. ERIK OBERG, *Machinery's Handbook, 29th Edition* (pp. 637-648). New York: INDUSTRIAL PRESS.

John. (2011, April 11). *Central Coast Climbing*. Retrieved May 17, 2013, from Blogspot: http://centralcoastclimbing.blogspot.com/2011/04/anchor-installment-2-trad.html

Puttock, M. J., & Thwaite, E. G. (1969). Elastic Compression of Spheres and Cylinders at Point and Line Contact. In M. J. Puttock, & E. G. Thwaite, *Elastic Compression of Spheres and Cylinders at Point and Line Contact* (p. 14). Melbourne: Commonwealth Scientific and Industrial.

Sam. (2012, May 4). *The Tangent Season*. Retrieved May 17, 2013, from Blogspot: http://thetangentseason.blogspot.com/

Slocum, D. A. (2007). Pappalardo Professor of Mechanical Engineering. In D. A. Slocum, *FUNdaMENTALS™ of Design* (pp. "9-15"-"9-17"). Cambridge: Massachusetts Institute of Technology.